FULL PAPER

ADVANCED
ENGINEERING
MATERIALS

www.aem-journal.com

Check for
updates

Fiber Volume Fraction Influence on Randomly Distributed Short Fiber Tungsten Fiber-Reinforced Tungsten Composites

Yiran Mao,* Jan W. Coenen, Johann Riesch, Sree Sistla, Jürgen Almanstötter, Alexis Terra, Chang Chen, Yucheng Wu, Leonard Raumann, Till Höschen, Hanns Gietl, Rudolf Neu, Christoph Broeckmann, and Christian Linsmeier

For future fusion reactors, tungsten (W) is currently the main candidate for the application as plasma-facing material due to its several advanced properties. To overcome the brittleness of W, randomly distributed short W fiber-reinforced W (W_f/W) composites have been developed using field-assisted sintering technology (FAST). Herein, W_f/W materials with different fiber volume fraction (20–60%) are manufactured by FAST process to study the fiber volume fraction influence on the composite properties. W_f/W with ductile fibers and brittle fibers is produced using different tool setups during the production. Three-point bending tests on prenotched samples, 4-point bending tests, and tensile tests have been performed to determine the fracture behavior and flexural/tensile strength of the material. W_f/W materials with 30–40% fiber volume fraction exhibit a promising pseudoductile behavior, similar to fiber-reinforced ceramic composites. However, W_f/W with 20% and >50% fiber volume fraction shows only a limited extrinsic toughening effect. In terms of flexural strength, with increasing fiber volume fraction, the tensile/flexural strength does not show a clear increasing tendency, or even lightly decreases.

1. Introduction

For future fusion reactors, tungsten (W) is currently the main candidate for the application as plasma-facing material as it is resilient against erosion, has the highest melting point of any metal, and shows rather benign behavior under neutron irradiation.[1–3] However, a major concern of W is its intrinsic brittleness under the extreme fusion environment with high transient heat loads and neutron irradiation.[4] Cracks could be formed and lead to a component failure. To overcome this drawback, W fiber-reinforced W (W_f/W) composites have been developed.[5–9] Relying on an extrinsic toughening principle, even in the brittle regime, this material allows for a certain tolerance toward cracking and damage in general in comparison to conventional W.[5,10–14] In general, similar to the ceramic fiber-reinforced composites, a relatively weak interface between the fiber and the matrix is considered to be beneficial to achieve the so-called pseudoductility.[10,13,15–17]

In previous studies, the W_f/W material is mainly produced by chemical vapor deposition (CVD) process.[9,14,18,19] However, powder metallurgy (PM) processes are the main manufacturing routes to produce W material in industry. Compared with the CVD process, PM processes have several benefits, such as substantial experience with bulk production, higher production rate, and an easier realization of alloyed materials. In recent studies,

Dr. Y. Mao, Dr. J. W. Coenen, A. Terra, L. Raumann, Prof. C. Linsmeier
Institut für Energie-und Klimaforschung - Plasmaphysik
Partner in the Trilateral Euregio Cluster
Forschungszentrum Jülich GmbH
Jülich 52425, Germany
E-mail: y.mao@fz-juelich.de

Dr. Y. Mao, Dr. C. Chen, Prof. Y. Wu
School of Materials Science and Engineering
Hefei University of Technology
Hefei 230009, China

ⓘ The ORCID identification number(s) for the author(s) of this article can be found under https://doi.org/10.1002/adem.201901242.

Dr. J. Riesch, T. Höschen, Dr. H. Gietl, Prof. R. Neu
Division Plasma Edge and Wall
Max-Planck-Institut für Plasmaphysik
Garching bei München 85748, Germany

S. Sistla, Prof. C. Broeckmann
Institut für Werkstoffanwendungen im Maschinenbau (IWM)
RWTH Aachen University
Aachen 52062, Germany

Dr. J. Almanstötter
AM Development Metal
OSRAM GmbH
SP PRE PLM DMET
Mittelstetter Weg 2, Schwabmünchen 86830, Germany

a process using field-assisted sintering technology (FAST) to produce W_f/W composite has been established.[5,10,11,20] As it is technically difficult to introduce aligned long fibers into the bulk material like the CVD process, short fibers with random distribution are used to realize the reinforcement in the FAST process.

Fiber volume fraction is often concerned as a crucial factor in typical ceramic fiber-reinforced composites.[21] Generally, large fiber volume fraction will increase the composite strength due to the advanced properties of fibers.[22–24] To have an efficient reinforcement, a critical fiber volume fraction needs to be reached so that when matrix fails, the fibers themselves can still withstand the load, otherwise a catastrophic failure could happen. However, if the fiber volume fraction is too high, so that the fiber spacing is less than a minimum value, the structure will collapse due to shear failure.[21,23,25–27] Also from the manufacturing point of view, a high volume fraction will cause challenges in terms of fiber/powder mixing homogeneity, fiber/powder mixture flowability, and sintering homogeneity.

For CVD-produced W_f/W, aligned long fibers are used for the reinforcement. When the load is directed along the fibers, the mechanical properties should increase with increasing fiber volume fraction.[8] However, for PM-produced W_f/W with randomly distributed short fibers, the fiber structure leads to a significant difference with respect to the fracture behavior compared with CVD W_f/W. Therefore, the influence of the fiber volume fraction on the composite properties remains unclear and an optimized fiber volume fraction for the PM produced W_f/W needs to find out with current fiber structure and geometry.

In this work, W_f/W with randomly distributed short fibers have been produced with various fiber volume fraction by FAST process. A series of mechanical tests have been performed to reflect the mechanical property changes related to different fiber volume fractions.

2. Experimental Section

2.1. Composite Manufacturing

Pure W powders (OSRAM GmbH) with 5 μm average particle size (Fisher Sub Sieve Sizer) and potassium-doped short W fibers (OSRAM GmbH) with 2.4 mm length and 0.15 mm diameter were the raw material for the composite manufacturing. The W fibers were produced by a drawing process and then cut into the required length. Due to the elongated drawing grain structure, the W fibers showed ductile behavior and extremely high tensile strength ($\approx$3000 MPa).[28] The potassium doping was used to reduce the grain coursing at high temperature. Potassium was insoluble in W; the doping (approximately 60–75 ppm) was present in the form of nanodispersed bubble rows along the elongated grains pinning the grain boundaries. It led to a good high-temperature microstructural stability compared with normal W fibers.[29]

The W fibers were coated with yttrium oxide as an interface layer before the consolidation process. The fibers were cleaned in isopropanol using ultrasonic bath for 10 min before coating with yttria. Based on the scanning electron microscope (SEM) observation with energy-dispersive X-ray spectroscopy (EDS), after cleaning the fibers, there were no visible oxide layers on top of the fibers. Only pure W signal can be detected. The yttria coating thickness was $\approx$2 μm. The coating was realized by a four-step process using magnetron sputtering similar to ref. [10]. Afterward, the coated fibers were mixed with the W powders by manual shaking in a vessel with various fiber mass fractions from 20% to 60%. The mixture was then poured into the graphite FAST mold. The sintering tool system (**Figure 1**) that is used in this study was similar to the one used in ref. [11]: 1) graphite sheets were placed between the mold and mixture, aiming to reduce the damage of the punch surface and to ease sample removal after the FAST process (Figure 1 left); 2) to separate the powder–fiber mixture and the graphite mold, W foils with 25 μm thickness were used, to reduce the carbon contamination of the W fibers (Figure 1 right).

The consolidation process was established by a FAST system (HP D 25-2) from "FCT Systeme GmbH." The sample was firstly heated up to 1900 °C (the temperature was measured at the bottom of the semihollow punch) with a constant heating rate of 200 °C min^{-1}. Then the temperature was hold for 4 min under a constant pressure of 60 MPa.[30,31] The external pressure applied on the powder compact was limited by the strength of the graphite die material. The sintering was performed in vacuum below 0.1 mbar. During the cooling stage, the average
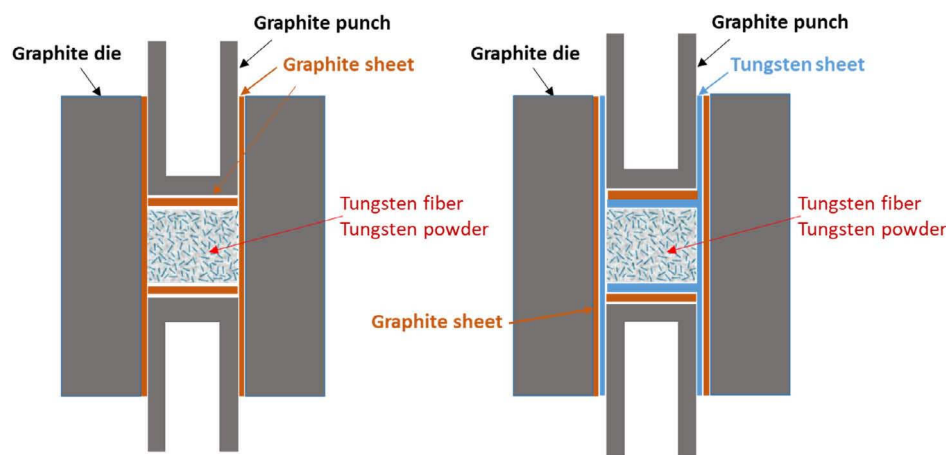
Figure 1. Mold system that used during FAST process. Left: mold without W foil protection; right: mold with W foil protection.

ADVANCED
SCIENCE NEWS
www.advancedsciencenews.com

ADVANCED
ENGINEERING
MATERIALS
www.aem-journal.com

cooling rate between 1900 and 400 °C was ≈375 °C min^{-1}. As a result, coin-shaped samples (20 mm diameter and ≈5 mm height) were produced similar to refs. [5,10].

These two different mold designs will lead to different fiber properties after FAST process. In previous studies,[11,32,33] it had been reported that under the high temperature during FAST process (≈1900 °C for 4 min), the W fibers were prone to be embrittled. Indeed, the elevated temperature during FAST process will cause fiber recrystallization and grain growth.[10] However, based on the study in ref. [14], the potassium-doped W fibers could remain ductile even after annealing at 2000 °C for 30 min. The heating condition in FAST process was lower than that. This phenomenon gave us a hint that this degradation of the fiber ductility was also caused by impurities because our sample was in direct contact with the graphite mold during the FAST process, and it had been investigated in a previous study that C impurities could increase the ductile–brittle transition temperature (DBTT) of W.[34] Therefore, in later cases, an additional layer of W foil was used to separate the W sample and the graphite mold. With W foil protection, no significant change could be detected in terms of microstructure, but the fibers started to show ductile behavior.[11] The average carbon concentration in the W fiber was difficult to analysis, as to separate the fiber and the matrix after sintering was quite challenging. The overall carbon content in the W$_f$/W was neglectable based on a combustion test. This means the carbon impurities were segregated in the W fibers. This effect could be caused by the carbon which was interacted with the high density of dislocations.[33] The carbon impurities were detected in fibers by a transmission electron microscopy (TEM) analysis. The embrittlement was caused largely by a carbide layer formation at the grain boundaries because the fiber ductile deformation was mainly realized by grain boundary sliding. With a W foil protection, such carbides formation was not anymore detectable. In this article, the "brittle" and "ductile" fibers refer to the samples not protected by W foil and protected by W foil during FAST process, respectively.[33]

2.2. Mechanical Testing

A 3-point bending test on notched samples (at room temperature [RT]) was chosen to investigate the fracture behavior similar to ref. [10]. Sample dimensions were $18 \times 2 \times 4$ mm^3 (length × width × thickness, manufactured by diamond wire cutting) with a ≈2 mm deep notch. The prenotch for 3-point bending test was prepared by diamond wire cutting with wire diameter of 0.04 mm (GS-1000 wire cutting machine from company Sommer Präzisionstechnik) followed by manually razor blade polishing for 3 min. The sample configuration and the prepared prenotch are shown in **Figure 2**.

The 3-point bending test was performed using an Instron 3342 universal testing machine together with a 3-point bending pin system 2810-400 (from Instron GmbH). The pin roller diameter was 2 mm. During the test, the sample was set on two support pins with a distance of 16 mm, and compressed by a load pin in the middle. The pin moved with a constant speed during the test (0.3 mm min^{-1}), and the corresponding pressing force applied on the load pin was recorded. Force–displacement curves could be generated until the sample failure, from which a fracture propagation behavior could be analyzed. The displacement measured represented the machine load pin displacement, which included the stiffness of all testing machine components. As consequence, this measurement gave only qualitative data.

Four-point bending tests were performed to measure the flexural strength at RT. The 4-point bending test sample dimension was $20 \times 2 \times 2.25$ mm^3 (length × width × thickness). The sample geometry was manufactured by diamond wire cutting similar to the 3-point bending samples.

During the test, the samples were placed on two support pins with a distance of 18 mm. A pressing load from two load pins with a distance of 9 mm was applied in the middle of the sample. The load pins move with a constant speed of 0.3 mm min^{-1} during the test. The maximum force of the test was recorded as the fracture force F. From this result, the flexural strength can be calculated[35]

$$\sigma_{\text{flexural}} = \frac{3FL_b}{4b_b h_b^2} \tag{1}$$

where σ_{flexural} is the flexural strength of the sample; F_b is the maximum force; L_b is the distance between the two support pins; b_b is the width of the sample; and h_b is the height of the sample.

To measure the tensile strength of the W$_f$/W material, a tensile test was also performed at RT. Dog-bone shape samples with a gauge length of 4.71 mm and a cross section of 2×2 mm^2 were used. The sample geometry was manufactured by electrical discharged machining (EDM).

The tensile tests were performed using a universal testing device (TIRAtest 2820, Nr. R050/01, TIRA GmbH). The force
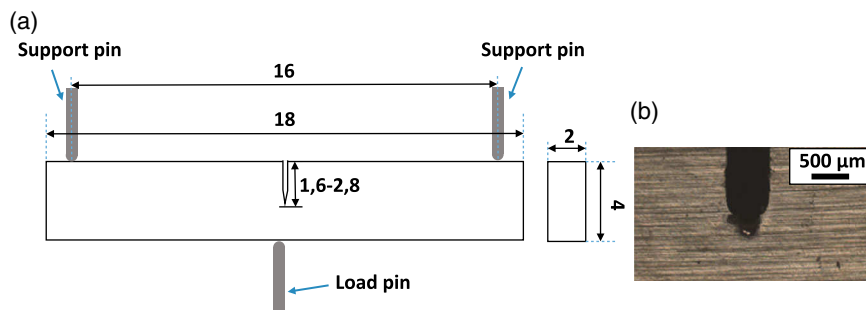
Figure 2. a) A 3-point bending sample configuration; b) prenotch prepared by diamond wire cutting and razor blade polishing.

**ADVANCED
SCIENCE NEWS**
www.advancedsciencenews.com

**ADVANCED
ENGINEERING
MATERIALS**
www.aem-journal.com

was recorded by a 20 kN load cell. A specially designed holding system was used to avoid stress peaks at the contact surface of the holder and the specimen. Moreover, the holders were mounted with a chain system to the grip of the testing device to ensure self-alignment and thus a uniaxial stress-state within the specimen.

Each specimen was preloaded with 20 N. The test was conducted with a constant displacement rate of 5 μm s^{-1}. The maximum tensile force before sample failure was recorded. Then the tensile strength $\sigma_{tensile}$ could be calculated by

$$\sigma_{tensile} = \frac{F_t}{b_t h_t} \qquad (2)$$

where F_t is the maximum tensile force, b_t is the width of the sample (2 mm), and h_t is the thickness of the sample (2 mm). In this work, the tensile test is performed only for W$_f$/W with brittle fibers.

3. Results

3.1. Microstructure and Sample Density

The microstructure of the W$_f$/W samples is investigated. As an example, the microstructures of the 20% and 50% fiber volume fraction W$_f$/W are shown in **Figure 3**, together with a typical microstructure of the fiber/interface area.

No major defect can be observed in both cases. The microstructure is similar to previous studies:[5,10,11] the fiber

distributions are rather random. Fiber deformation can be observed. Between fiber and matrix, the yttria interface is visible. However, the yttria interface got damaged during the FAST process due to the high temperature and external pressure, especially the outer shell. Pores are visible in the matrix. They are relatively small and distributed homogeneously in the matrix. The average grain size of the matrix is around 5 μm. About the microstructure of the fibers, high temperature will cause fiber recrystallization and grain growth, as shown in ref. [10]. With W foil protection, no significant change can be detected in terms of fiber microstructure compared with the sample produced with graphite foil, as shown in ref. [11]. The relative density of the samples is shown in **Table 1**. The density increases slightly with increasing fiber volume fraction because of the increasing fraction of the already-dense fibers.

3.2. Fracture Behavior and Strength

The force–displacement curves of prenotched 3-point bending tests for W$_f$/W with brittle fibers ductile fibers are shown in **Figure 4** and **5**, respectively. It is important to note that the absolute values of the force and displacement 3-point bending curves are not directly comparable because the prenotch is manually prepared, and therefore the sharpness and the depth of the notches are quite scattered. However, the main aim of this test is to observe the crack propagation behavior of the samples with precracks.
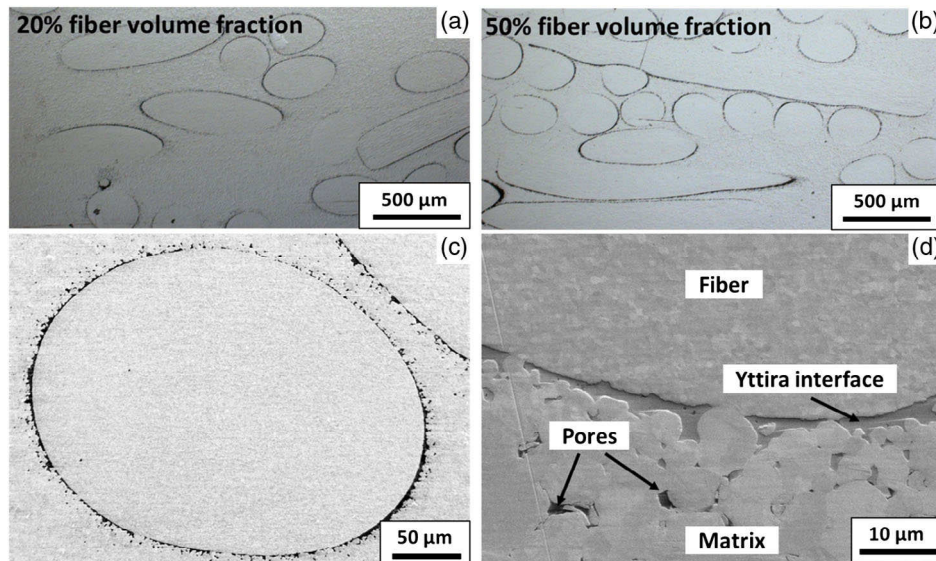

Figure 3. LM images showing overview microstructures of W$_f$/W with a) 20% and b) 50% fiber volume fractions W$_f$/W; c,d) SEM images showing microstructure of the fiber/interface area of typical W$_f$/W composites.

Table 1. Relative density of the FAST-produced W$_f$/W with different fiber volume fraction.

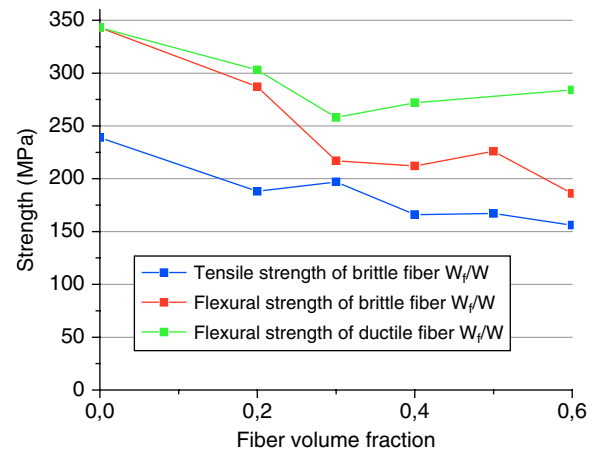| Density	20% Fiber	30% Fiber	40% Fiber	50% Fiber	60% Fiber
W$_f$/W with brittle fibers	≈93.3 ± 0.8%	≈94.2 ± 0.1%	≈94.0 ± 0.2%	≈94.1 ± 0.1%	≈94.6 ± 0.5%
W$_f$/W with ductile fibers	≈91.2 ± 0.5%	≈92.3 ± 0.9%	≈92.8 ± 0.2%	–	≈93.7 ± 0.6%

1901242 (4 of 8)
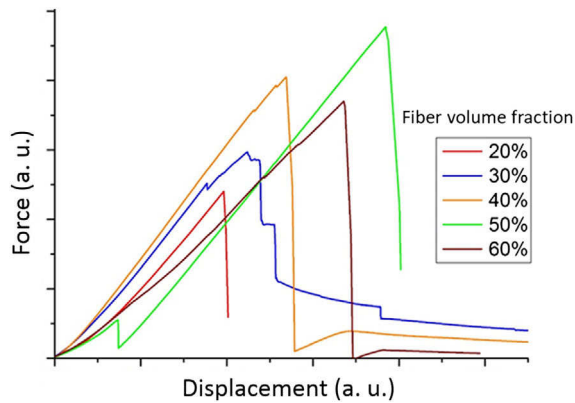
Figure 4. Prenotched 3-point bending test load–displacement curves of brittle fiber W_f/W with different fiber volume fraction.
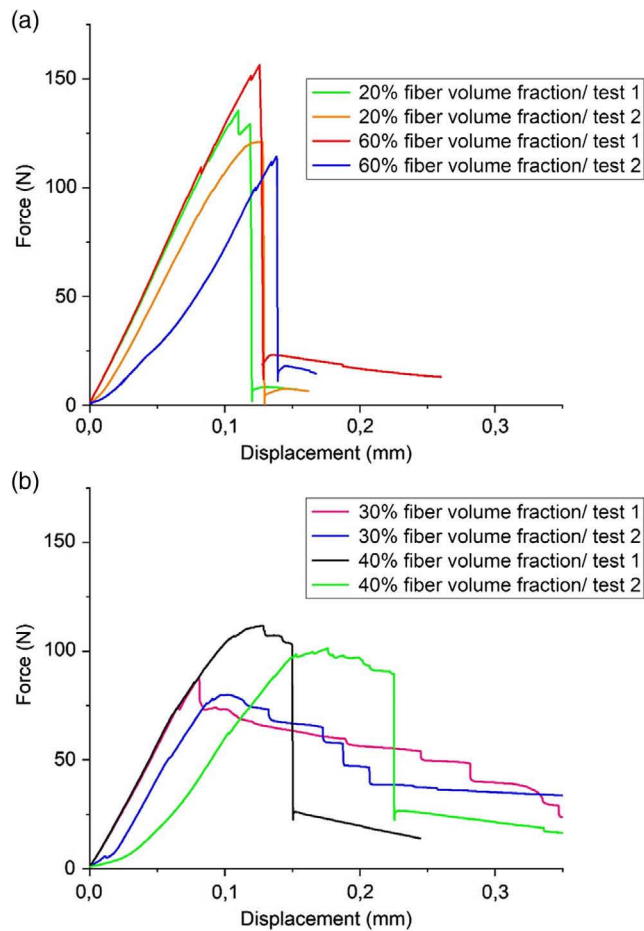
Figure 5. Force–displacement curves of prenotched 3-point bending test on ductile fiber W_f/W with a) 20% and 60% fiber volume fractions and b) 30% and 40% fiber volume fractions.

Figure 6. Tensile strength and flexural strength of FAST-produced pure W_f/W with different fiber volume fractions.

As shown in Figure 4, for the brittle fiber case, W_f/W with 20% fiber volume fraction shows pure elastic brittle fracture. For the sample with 30% fiber volume fraction, a typical pseudoductile curve can be observed similar to previous studies:[3,5,10,11] the first load-drop marks the matrix failure;

after tits failure, the load still increases due to the crack bridging by the fibers; the interface's gradual debonding let the material establish a stable crack opening before the maximum force; the massive load-drop after the maximum load indicates unstable crack propagation; after which the stepwise load bearing capability is probably supplied by frictional fiber pull-out from the matrix. Here, the fiber elastic bridging, interface debonding, crack deflection, and fiber pull-out are likely the energy dissipation mechanisms which contribute to the elevated fracture resistance compared with pure W.[12,36] However, with a fiber volume fraction larger than 30%, only limited fracture resistance can be achieved after the matrix failure. These samples show quite sudden load-drop after reaching the maximum load.

For the ductile fiber case (Figure 5), each type of sample is measured twice. For the 20% and 60% case, further load increasing can be observed after the matrix failure. However, the defect tolerance is quite low due to the rather sudden load-drop after the maximum loading. A stepwise/continuous load decreasing is not observed. For the samples with 30% and 40% fiber volume fraction, typical pseudoductile behavior is performed with rising load capability after precrack and non-catastrophic failure.

The flexural/tensile strength values of W_f/W with different fiber volume fractions are shown in **Figure 6**. With increasing fiber volume fraction, the tensile/flexural strengths do not show a clear increasing tendency, or even slightly decreases.

After the mechanical testing, the fracture surfaces are investigated by SEM. The prenotched 3-point bending test and tensile test fracture sections of the 30% and 60% fiber volume fraction samples are shown in **Figure 7** and **8** as examples.

From Figure 7, the proper interface debonding and fiber ductile deformation, fiber pull-out effects can be observed only for the sample with 30% fiber volume fraction.[10,11] For the 60% fiber sample, such effects are not visible.

4. Discussion

For the 20% fiber volume fraction cases, the likely reason for the limited pseudoductility is that the composite does not contain
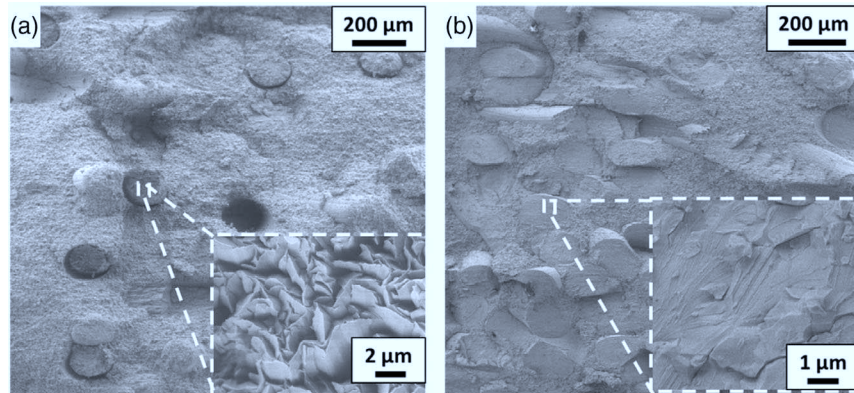
Figure 7. SEM image of the fracture section of ductile fiber W_f/W with a) 30% and b) 60% fiber volume fraction after the prenotched 3-point bending test.
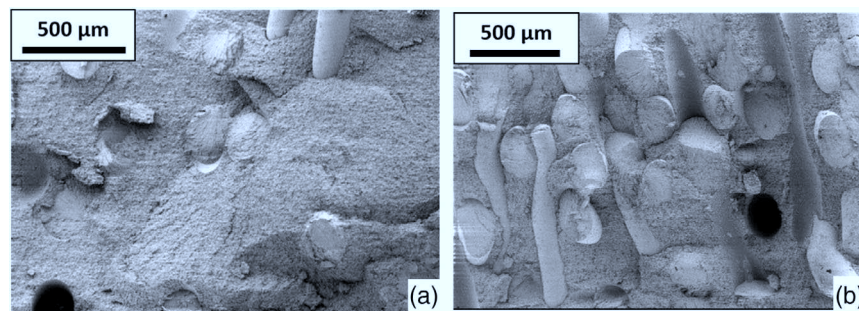

Figure 8. SEM image of the fracture section of W_f/W with a) 30% and b) 60% fiber volume fractions after the tensile test.

enough fibers. Consequently, the crack front could not be bridged efficiently, and later on, only limited fiber pull-out could perform. Without these energy dissipation mechanisms, the defect tolerance could not increase.

For the very high fiber volume fraction cases (>50%), the composite crack opening could be largely influenced by the weak interface failure before matrix cracking, as discussed in ref. [7,10]. As shown in **Figure 9**, during the crack opening, with the increasing loading, the weak interface tends to be predamaged before matrix failure. When the crack front encounters the predamaged area, the unstable crack opening could appear. In addition, a substantial number of predamages could lead to the formation of a new crack source and for very high fiber volume fraction, the crack front has a higher chance to meet an already damaged interface. All of these effects could cause an unstable crack growth with a sudden load drop, which means that the pseudoductility of the high fiber volume fraction (>50%) W_f/W is quite limited.

Figure 7a shows a typical ductile fiber fracture surface of the 30% W_f/W. The ductility of the fibers can be distinguished by the fracture surface. For ductile fibers, the fracture surface gives a pattern with knife edge shape. The knife edge shape pattern could be caused by the grain boundary sliding of the elongated grains. Also, the fiber diameter will be locally reduced due to the so-called necking effect. In contrast, for the 60% case (Figure 7a), the fracture surfaces give a brittle cleavage failure with characteristic river line pattern. The fiber diameter
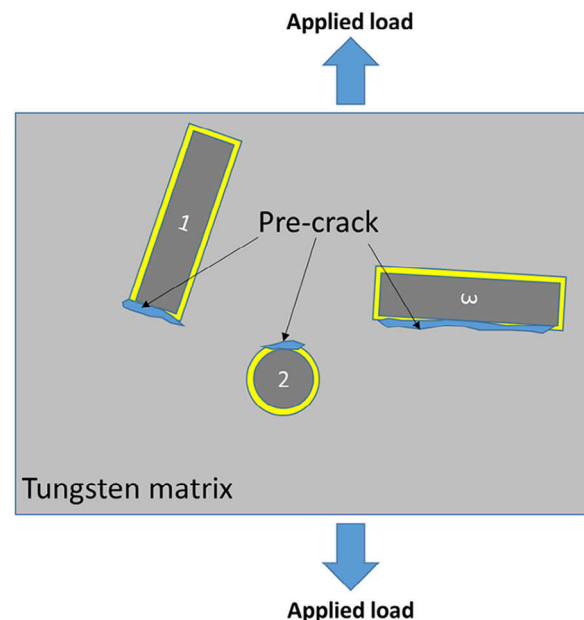
Figure 9. Weak yttria interface failure under loading condition before matrix failure.

is also not locally reduced. This brittle fiber failure could be caused by the high local strain rates during the unstable

**ADVANCED
SCIENCE NEWS**

www.advancedsciencenews.com

**ADVANCED
ENGINEERING
MATERIALS**

www.aem-journal.com

cracking, which could inhibit the ductile deformation of the W fiber.[37,38]

Generally, the strength should increase linearly with the increasing fiber volume fraction, according to refs. [21,26]:

$$\sigma_c = \sigma_f \nu_f + \sigma_m \nu_m \qquad (3)$$

where σ_c is the strength of the composite; σ_f and σ_m are the strength of the fiber and the matrix, respectively; and ν_f and ν_m are the volume fraction of the fiber and the matrix.

However, for FAST-produced W_f/W with increasing fiber volume fraction, the tensile/flexural strength slightly decreases, as shown in Figure 6. This could be explained by the fact that the composite strength is again dominated by the weak interface existence for the random distributed short fiber case, as reported in ref. [10]. The weak interface positions will form predamage before the matrix failure under high load. With increasing fiber volume fraction, the weak interface areas are enlarged. Therefore, the increasing fiber volume fraction will weaken the composite strength by introducing more potential predamage positions. As can be deduced from Figure 8b, the fracture surface of the 60% fiber volume fraction W_f/W exposes many interface areas, which implies that the superior fiber strength cannot contribute to the composite strength. This is a particular issue for the random discontinuous W_f/W composites because of the existence of the fiber ends and the fibers being vertically oriented to the loading direction.

These interpretations are made based only on a quite limited number of experiments. However, they seem to indicate that the random distribution of the reinforcing fibers has great influence on the crack behavior and the composite strength properties. These assorted behavior and mechanisms could lead to different design rules compared with the ones deduced from the studies on the CVD W_f/W material with aligned long fibers.

5. Conclusion

W_f/W with different fiber volume fraction has been produced and studied. With too low ($\approx$20%) or too high ($>$50%) fiber volume fraction, efficient pseudoductility cannot be established due to the randomly distributed and oriented fibers. In addition, with increasing fiber volume fraction, the tensile/flexural strength does not show an increasing tendency. This is because the higher fiber volume fraction introduces more weak interface positions, which could potentially form predamage during the load. Based on the above tests, $\approx$30–40% would be regarded as the optimized fiber volume fraction with the current W_f/W design.

Acknowledgements

Conflict of Interest

The authors declare no conflict of interest.

Keywords

[1] I. Smid, M. Akiba, G. Vieider, L. Plöchl, *J. Nucl. Mater.* **1998**, *258263*, 160.

[2] V. Philipps, *J. Nucl. Mater.* **2011**, *415*, S2.

[3] J. W. Coenen, S. Antusch, M. Aumann, W. Biel, J. Du, J. Engels, S. Heuer, A. Houben, T. Hoeschen, B. Jasper, F. Koch, J. Linke, A. Litnovsky, Y. Mao, R. Neu, G. Pintsuk, J. Riesch, M. Rasinski, J. Reiser, M. Rieth, A. Terra, B. Unterberg, W. Th, T. Wegener, J. H. You, L. Ch, *Phys. Scr.* **2016**, *2016*, 014002.

[4] G. Pintsuk, I. Bobin-Vastra, S. Constans, P. Gavila, M. Rödig, B. Riccardi, *Fusion Eng. Des.* **2013**, *88*, 1858.

[5] Y. Mao, J. W. Coenen, J. Riesch, S. Sistla, J. Almanstötter, B. Jasper, A. Terra, T. Höschen, H. Gietl, M. Bram, J. Gonzalez-Julian, C. Linsmeier, C. Broeckmann, *Phys. Scr.* **2017**, *T170*, 014005.

[6] Y. Mao, J. Engels, A. Houben, M. Rasinski, J. Steffens, A. Terra, C. Linsmeier, J. W. Coenen, *Nucl. Mater. Energy* **2017**, *10*, 1.

[7] Y. Mao, J. W. Coenen, J. Riesch, S. Sistla, J. Almanstötter, J. Reiser, A. Terra, C. Chen, Y. Wu, L. Raumann, T. Höschen, H. Gietl, R. Neu, C. Linsmeier, C. Broeckmann, *Nucl. Fusion* **2019**, *59*, 086034.

[8] H. Gietl, A. von Muller, J. W. Coenen, M. Decius, D. Ewert, T. Hoschen, P. Huber, M. Milwich, J. Riesch, R. Neu, *J. Compos. Mater.* **2018**, *52*, 3875.

[9] J. Riesch, T. Hoschen, C. Linsmeier, S. Wurster, J. H. You, *Phys. Scr.* **2014**, *T159*, 014031.

[10] Y. Mao, J. W. Coenen, J. Riesch, S. Sistla, J. Almanstotter, B. Jasper, A. Terra, T. Hoschen, H. Gietl, C. Linsmeier, C. Broeckmann, *Composites A* **2018**, *107*, 342.

[11] J. W. Coenen, Y. Mao, S. Sistla, J. Riesch, T. Hoeschen, C. Broeckmann, R. Neu, C. Linsmeier, *Nucl. Mater. Energy* **2018**, *15*, 214.

[12] J. Riesch, J. Y. Buffiere, T. Höschen, M. di Michiel, M. Scheel, C. Linsmeier, J. H. You, *Acta Mater.* **2013**, *61*, 7060.

[13] H. Gietl, J. Riesch, J. W. Coenen, T. Hoschen, C. Linsmeier, R. Neu, *Fusion Eng. Des.* **2017**, *124*, 396.

[14] J. Riesch, Y. Han, J. Almanstotter, J. W. Coenen, T. Hoschen, B. Jasper, P. Zhao, C. Linsmeier, R. Neu, *Phys. Scr.* **2016**, *T167*, 014006.

[15] G. Czél, M. R. Wisnom, *Composites A* **2013**, *52*, 23.

[16] H. Ming-Yuan, J. W. Hutchinson, *Int. J. Solids Struct.* **1989**, *25*, 1053.

[17] S. Schönen, B. Jasper, J. W. Coenen, J. Du, T. Höschen, J. Riesch, G. Natour, R. Neu, C. Linsmeier, *Compos. Interfaces* **2018**, *26*, 107.

[18] R. Neu, J. Riesch, J. W. Coenen, J. Brinkmann, A. Calvo, S. Elgeti, C. García-Rosales, H. Greuner, T. Hoeschen, G. Holzner, F. Klein, F. Koch, C. Linsmeier, A. Litnovsky, T. Wegener, S. Wurster, J. H. You, *Fusion Eng. Des.* **2016**, *109111*, 1046.

[19] J. Du, T. Höschen, M. Rasinski, S. Wurster, W. Grosinger, J. H. You, *Compos. Sci. Technol.* **2010**, *70*, 1482.

[20] J. W. Coenen, Y. Mao, J. Almanstotter, A. Calvo, S. Sistla, H. Gietl, B. Jasper, J. Riesch, M. Rieth, G. Pintsuk, F. Klein, A. Litnovsky, A. V. Mueller, T. Wegener, J. H. You, C. Broeckmann, C. Garcia-Rosales, R. Neu, C. Linsmeier, *Fusion Eng. Des.* **2017**, *124*, 964.

[21] A. Kelly, G. Davies, *Metall. Rev.* **1965**, *10*, 1.

[22] P. J. Hine, H. Rudolf Lusti, A. A. Gusev, *Compos. Sci. Technol.* **2002**, *62*, 1445.

[23] M. Mohamed, L. V. C. H. Toshiyuki, *J. Am. Ceram. Soc.* **1995**, *78*, 3369.

[24] S. Y. Fu, B. Lauke, E. Mäder, C. Y. Yue, X. Hu, *Composites A* **2000**, *31*, 1117.

[25] K. K. Chawla, *Composite Materials*, Springer, Berlin/New York **1998**, p. 212.

[26] V. Laws, *J. Phys. Appl. Phys.* **1971**, *4*, 1737.

[27] N. Pan, *Polym. Compos.* **1993**, *14*, 85.

[28] P. Zhao, J. Riesch, T. Hoschen, J. Almanstotter, M. Balden, J. W. Coenen, R. Himml, W. Pantleon, U. von Toussaint, R. Neu, *Int. J. Refract. Met. Hard Mater.* **2017**, *68*, 29.

[29] C. L. Briant, O. Horacsek, K. Horacsek, *Metall. Trans. A* **1993**, *24*, 843.

[30] S. Chanthapan, A. Kulkarni, J. Singh, C. Haines, D. Kapoor, *Int. J. Refract. Met. Hard Mater.* **2012**, *31*, 114.

[31] K. C. Cho, R. H. Woodman, B. R. Klotz, R. J. Dowding, *Mater. Manuf. Processes* **2004**, *19*, 619.

[32] A. V. Müller, M. Ilg, H. Gietl, T. Höschen, R. Neu, G. Pintsuk, J. Riesch, U. Siefken, J. H. You, *Nucl. Mater. Energy* **2018**, *16*, 163.

[33] Y. Mao, C. Chen, J. W. Coenen, J. Riesch, S. Sistla, J. Almanstötter, A. Terra, Y. Wu, L. Raumann, T. Höschen, H. Gietl, R. Neu, C. Linsmeier, C. Broeckmann, *Fusion Eng. Des.* **2019**, *145*, 18.

[34] J. R. Stephens. *Effects of Interstitial Impurities on the Low-Temperature Tensile Properties of Tungsten*, National Aeronautics and Space Administration Cleveland OH Lewis Research Center, United States **1964**.

[35] W. H. Dietmar Gross, J. Schröder, W. A. Wall, *Technische Mechanik, Vol. 2: Elastostatik*, Springer, Berlin, Heidelberg **2009**.

[36] H. Stang, S. P. Shah, *J. Mater. Sci.* **1986**, *21*, 953.

[37] D. Rupp, S. M. Weygand, *J. Nucl. Mater.* **2011**, *417*, 477.

[38] A. Giannattasio, S. G. Roberts, *Philos. Mag.* **2007**, *87*, 2589.

1901242 (8 of 8)